

$Z\gamma$ Production in $p\bar{p}$ Collisions at $\sqrt{s} = 1.8$ TeV and Limits on Anomalous $ZZ\gamma$ and $Z\gamma\gamma$ Couplings

The DØ Collaboration*

Fermi National Accelerator Laboratory, Batavia, IL 60510

(October 29, 1997)

Abstract

We present a study of $Z\gamma + X$ production in $p\bar{p}$ collisions at $\sqrt{s} = 1.8$ TeV from 97 (87) pb^{-1} of data collected in the $ee\gamma$ ($\mu\mu\gamma$) decay channel with the DØ detector at Fermilab. The event yield and kinematic characteristics are consistent with the Standard Model predictions. We obtain limits on anomalous $ZZ\gamma$ and $Z\gamma\gamma$ couplings for form factor scales $\Lambda = 500$ GeV and $\Lambda = 750$ GeV. Combining this analysis with our previous results yields 95% CL limits $|h_{30}^Z| < 0.36$, $|h_{40}^Z| < 0.05$, $|h_{30}^\gamma| < 0.37$, and $|h_{40}^\gamma| < 0.05$ for a form factor scale $\Lambda = 750$ GeV.

* Authors listed on the following page.

Submitted to Physical Review Letters.

$Z\gamma$ Production in $p\bar{p}$ Collisions at $\sqrt{s} = 1.8$ TeV and Limits on Anomalous $ZZ\gamma$ and $Z\gamma\gamma$ Couplings

B. Abbott,³⁰ M. Abolins,²⁷ B.S. Acharya,⁴⁵ I. Adam,¹² D.L. Adams,³⁹ M. Adams,¹⁷
S. Ahn,¹⁴ H. Aihara,²³ G.A. Alves,¹⁰ E. Amidi,³¹ N. Amos,²⁶ E.W. Anderson,¹⁹ R. Astur,⁴⁴
M.M. Baarmand,⁴⁴ A. Baden,²⁵ V. Balamurali,³⁴ J. Balderston,¹⁶ B. Baldin,¹⁴
S. Banerjee,⁴⁵ J. Bantly,⁵ E. Barberis,²³ J.F. Bartlett,¹⁴ K. Bazizi,⁴¹ A. Belyaev,²⁸
S.B. Beri,³⁶ I. Bertram,³³ V.A. Bezzubov,³⁷ P.C. Bhat,¹⁴ V. Bhatnagar,³⁶
M. Bhattacharjee,¹³ N. Biswas,³⁴ G. Blazey,³² S. Blessing,¹⁵ P. Bloom,⁷ A. Boehnlein,¹⁴
N.I. Bojko,³⁷ F. Borchering,¹⁴ C. Boswell,⁹ A. Brandt,¹⁴ R. Brock,²⁷ A. Bross,¹⁴
D. Buchholz,³³ V.S. Burtovoi,³⁷ J.M. Butler,³ W. Carvalho,¹⁰ D. Casey,⁴¹ Z. Casilum,⁴⁴
H. Castilla-Valdez,¹¹ D. Chakraborty,⁴⁴ S.-M. Chang,³¹ S.V. Chekulaev,³⁷ L.-P. Chen,²³
W. Chen,⁴⁴ S. Choi,⁴³ S. Chopra,²⁶ B.C. Choudhary,⁹ J.H. Christenson,¹⁴ M. Chung,¹⁷
D. Claes,²⁹ A.R. Clark,²³ W.G. Cobau,²⁵ J. Cochran,⁹ W.E. Cooper,¹⁴ C. Cretsinger,⁴¹
D. Cullen-Vidal,⁵ M.A.C. Cummings,³² D. Cutts,⁵ O.I. Dahl,²³ K. Davis,² K. De,⁴⁶
K. Del Signore,²⁶ M. Demarteau,¹⁴ D. Denisov,¹⁴ S.P. Denisov,³⁷ H.T. Diehl,¹⁴
M. Diesburg,¹⁴ G. Di Loreto,²⁷ P. Draper,⁴⁶ Y. Ducros,⁴² L.V. Dudko,²⁸ S.R. Dugad,⁴⁵
D. Edmunds,²⁷ J. Ellison,⁹ V.D. Elvira,⁴⁴ R. Engelmann,⁴⁴ S. Eno,²⁵ G. Eppley,³⁹
P. Ermolov,²⁸ O.V. Eroshin,³⁷ V.N. Evdokimov,³⁷ T. Fahland,⁸ M. Fatyga,⁴ M.K. Fatyga,⁴¹
S. Feher,¹⁴ D. Fein,² T. Ferbel,⁴¹ G. Finocchiaro,⁴⁴ H.E. Fisk,¹⁴ Y. Fisyak,⁷ E. Flattum,¹⁴
G.E. Forden,² M. Fortner,³² K.C. Frame,²⁷ S. Fuess,¹⁴ E. Gallas,⁴⁶ A.N. Galyaev,³⁷
P. Gartung,⁹ T.L. Geld,²⁷ R.J. Genik II,²⁷ K. Genser,¹⁴ C.E. Gerber,¹⁴ B. Gibbard,⁴
S. Glenn,⁷ B. Gobbi,³³ M. Goforth,¹⁵ A. Goldschmidt,²³ B. Gómez,¹ G. Gómez,²⁵
P.I. Goncharov,³⁷ J.L. González Solís,¹¹ H. Gordon,⁴ L.T. Goss,⁴⁷ K. Gounder,⁹
A. Goussiou,⁴⁴ N. Graf,⁴ P.D. Grannis,⁴⁴ D.R. Green,¹⁴ J. Green,³² H. Greenlee,¹⁴
G. Grim,⁷ S. Grinstein,⁶ N. Grossman,¹⁴ P. Grudberg,²³ S. Grünendahl,⁴¹ G. Guglielmo,³⁵
J.A. Guida,² J.M. Guida,⁵ A. Gupta,⁴⁵ S.N. Gurzhiev,³⁷ P. Gutierrez,³⁵ Y.E. Gutnikov,³⁷

N.J. Hadley,²⁵ H. Haggerty,¹⁴ S. Hagopian,¹⁵ V. Hagopian,¹⁵ K.S. Hahn,⁴¹ R.E. Hall,⁸
 P. Hanlet,³¹ S. Hansen,¹⁴ J.M. Hauptman,¹⁹ D. Hedin,³² A.P. Heinson,⁹ U. Heintz,¹⁴
 R. Hernández-Montoya,¹¹ T. Heuring,¹⁵ R. Hirosky,¹⁵ J.D. Hobbs,¹⁴ B. Hoeneisen,^{1,*}
 J.S. Hoftun,⁵ F. Hsieh,²⁶ Ting Hu,⁴⁴ Tong Hu,¹⁸ T. Huehn,⁹ A.S. Ito,¹⁴ E. James,²
 J. Jaques,³⁴ S.A. Jerger,²⁷ R. Jesik,¹⁸ J.Z.-Y. Jiang,⁴⁴ T. Joffe-Minor,³³ K. Johns,²
 M. Johnson,¹⁴ A. Jonckheere,¹⁴ M. Jones,¹⁶ H. Jöstlein,¹⁴ S.Y. Jun,³³ C.K. Jung,⁴⁴
 S. Kahn,⁴ G. Kalbfleisch,³⁵ J.S. Kang,²⁰ D. Karmgard,¹⁵ R. Kehoe,³⁴ M.L. Kelly,³⁴
 C.L. Kim,²⁰ S.K. Kim,⁴³ A. Klatchko,¹⁵ B. Klima,¹⁴ C. Klopfenstein,⁷ V.I. Klyukhin,³⁷
 V.I. Kochetkov,³⁷ J.M. Kohli,³⁶ D. Koltick,³⁸ A.V. Kostritskiy,³⁷ J. Kotcher,⁴
 A.V. Kotwal,¹² J. Kourlas,³⁰ A.V. Kozelov,³⁷ E.A. Kozlovski,³⁷ J. Krane,²⁹
 M.R. Krishnaswamy,⁴⁵ S. Krzywdzinski,¹⁴ S. Kunori,²⁵ S. Lami,⁴⁴ H. Lan,^{14,†} R. Lander,⁷
 F. Landry,²⁷ G. Landsberg,¹⁴ B. Lauer,¹⁹ A. Leflat,²⁸ H. Li,⁴⁴ J. Li,⁴⁶ Q.Z. Li-Demarteau,¹⁴
 J.G.R. Lima,⁴⁰ D. Lincoln,²⁶ S.L. Linn,¹⁵ J. Linnemann,²⁷ R. Lipton,¹⁴ Y.C. Liu,³³
 F. Lobkowicz,⁴¹ S.C. Loken,²³ S. Lökös,⁴⁴ L. Lueking,¹⁴ A.L. Lyon,²⁵ A.K.A. Maciel,¹⁰
 R.J. Madaras,²³ R. Madden,¹⁵ L. Magaña-Mendoza,¹¹ S. Mani,⁷ H.S. Mao,^{14,†}
 R. Markeloff,³² T. Marshall,¹⁸ M.I. Martin,¹⁴ K.M. Mauritz,¹⁹ B. May,³³ A.A. Mayorov,³⁷
 R. McCarthy,⁴⁴ J. McDonald,¹⁵ T. McKibben,¹⁷ J. McKinley,²⁷ T. McMahon,³⁵
 H.L. Melanson,¹⁴ M. Merkin,²⁸ K.W. Merritt,¹⁴ H. Miettinen,³⁹ A. Mincer,³⁰
 C.S. Mishra,¹⁴ N. Mokhov,¹⁴ N.K. Mondal,⁴⁵ H.E. Montgomery,¹⁴ P. Mooney,¹
 H. da Motta,¹⁰ C. Murphy,¹⁷ F. Nang,² M. Narain,¹⁴ V.S. Narasimham,⁴⁵ A. Narayanan,²
 H.A. Neal,²⁶ J.P. Negret,¹ P. Nemethy,³⁰ D. Norman,⁴⁷ L. Oesch,²⁶ V. Oguri,⁴⁰
 E. Oltman,²³ N. Oshima,¹⁴ D. Owen,²⁷ P. Padley,³⁹ M. Pang,¹⁹ A. Para,¹⁴ Y.M. Park,²¹
 R. Partridge,⁵ N. Parua,⁴⁵ M. Paterno,⁴¹ B. Pawlik,²² J. Perkins,⁴⁶ M. Peters,¹⁶
 R. Piegai,⁶ H. Piekarz,¹⁵ Y. Pischalnikov,³⁸ V.M. Podstavkov,³⁷ B.G. Pope,²⁷
 H.B. Prosper,¹⁵ S. Protopopescu,⁴ J. Qian,²⁶ P.Z. Quintas,¹⁴ R. Raja,¹⁴ S. Rajagopalan,⁴
 O. Ramirez,¹⁷ L. Rasmussen,⁴⁴ S. Reucroft,³¹ M. Rijssenbeek,⁴⁴ T. Rockwell,²⁷ N.A. Roe,²³
 P. Rubinov,³³ R. Ruchti,³⁴ J. Rutherford,² A. Sánchez-Hernández,¹¹ A. Santoro,¹⁰
 L. Sawyer,²⁴ R.D. Schamberger,⁴⁴ H. Schellman,³³ J. Sculli,³⁰ E. Shabalina,²⁸ C. Shaffer,¹⁵

H.C. Shankar,⁴⁵ R.K. Shivpuri,¹³ M. Shupe,² H. Singh,⁹ J.B. Singh,³⁶ V. Sirotenko,³²
W. Smart,¹⁴ R.P. Smith,¹⁴ R. Snihur,³³ G.R. Snow,²⁹ J. Snow,³⁵ S. Snyder,⁴ J. Solomon,¹⁷
P.M. Sood,³⁶ M. Sosebee,⁴⁶ N. Sotnikova,²⁸ M. Souza,¹⁰ A.L. Spadafora,²³
R.W. Stephens,⁴⁶ M.L. Stevenson,²³ D. Stewart,²⁶ F. Stichelbaut,⁴⁴ D.A. Stoianova,³⁷
D. Stoker,⁸ M. Strauss,³⁵ K. Streets,³⁰ M. Strovink,²³ A. Sznajder,¹⁰ P. Tamburello,²⁵
J. Tarazi,⁸ M. Tartaglia,¹⁴ T.L.T. Thomas,³³ J. Thompson,²⁵ T.G. Trippe,²³ P.M. Tuts,¹²
N. Varelas,²⁷ E.W. Varnes,²³ D. Vititoe,² A.A. Volkov,³⁷ A.P. Vorobiev,³⁷ H.D. Wahl,¹⁵
G. Wang,¹⁵ J. Warchol,³⁴ G. Watts,⁵ M. Wayne,³⁴ H. Weerts,²⁷ A. White,⁴⁶ J.T. White,⁴⁷
J.A. Wightman,¹⁹ S. Willis,³² S.J. Wimpenny,⁹ J.V.D. Wirjawan,⁴⁷ J. Womersley,¹⁴
E. Won,⁴¹ D.R. Wood,³¹ H. Xu,⁵ R. Yamada,¹⁴ P. Yamin,⁴ J. Yang,³⁰ T. Yasuda,³¹
P. Yepes,³⁹ C. Yoshikawa,¹⁶ S. Youssef,¹⁵ J. Yu,¹⁴ Y. Yu,⁴³ Z.H. Zhu,⁴¹ D. Zieminska,¹⁸
A. Zieminski,¹⁸ E.G. Zverev,²⁸ and A. Zylberstejn⁴²

(DØ Collaboration)

¹*Universidad de los Andes, Bogotá, Colombia*

²*University of Arizona, Tucson, Arizona 85721*

³*Boston University, Boston, Massachusetts 02215*

⁴*Brookhaven National Laboratory, Upton, New York 11973*

⁵*Brown University, Providence, Rhode Island 02912*

⁶*Universidad de Buenos Aires, Buenos Aires, Argentina*

⁷*University of California, Davis, California 95616*

⁸*University of California, Irvine, California 92697*

⁹*University of California, Riverside, California 92521*

¹⁰*LAFEX, Centro Brasileiro de Pesquisas Físicas, Rio de Janeiro, Brazil*

¹¹*CINVESTAV, Mexico City, Mexico*

¹²*Columbia University, New York, New York 10027*

¹³*Delhi University, Delhi, India 110007*

- ¹⁴*Fermi National Accelerator Laboratory, Batavia, Illinois 60510*
- ¹⁵*Florida State University, Tallahassee, Florida 32306*
- ¹⁶*University of Hawaii, Honolulu, Hawaii 96822*
- ¹⁷*University of Illinois at Chicago, Chicago, Illinois 60607*
- ¹⁸*Indiana University, Bloomington, Indiana 47405*
- ¹⁹*Iowa State University, Ames, Iowa 50011*
- ²⁰*Korea University, Seoul, Korea*
- ²¹*Kyungsoong University, Pusan, Korea*
- ²²*Institute of Nuclear Physics, Kraków, Poland*
- ²³*Lawrence Berkeley National Laboratory and University of California, Berkeley, California 94720*
- ²⁴*Louisiana Tech University, Ruston, Louisiana 71272*
- ²⁵*University of Maryland, College Park, Maryland 20742*
- ²⁶*University of Michigan, Ann Arbor, Michigan 48109*
- ²⁷*Michigan State University, East Lansing, Michigan 48824*
- ²⁸*Moscow State University, Moscow, Russia*
- ²⁹*University of Nebraska, Lincoln, Nebraska 68588*
- ³⁰*New York University, New York, New York 10003*
- ³¹*Northeastern University, Boston, Massachusetts 02115*
- ³²*Northern Illinois University, DeKalb, Illinois 60115*
- ³³*Northwestern University, Evanston, Illinois 60208*
- ³⁴*University of Notre Dame, Notre Dame, Indiana 46556*
- ³⁵*University of Oklahoma, Norman, Oklahoma 73019*
- ³⁶*University of Panjab, Chandigarh 16-00-14, India*
- ³⁷*Institute for High Energy Physics, 142-284 Protvino, Russia*
- ³⁸*Purdue University, West Lafayette, Indiana 47907*
- ³⁹*Rice University, Houston, Texas 77005*
- ⁴⁰*Universidade do Estado do Rio de Janeiro, Brazil*
- ⁴¹*University of Rochester, Rochester, New York 14627*

⁴²*CEA, DAPNIA/Service de Physique des Particules, CE-SACLAY, Gif-sur-Yvette, France*

⁴³*Seoul National University, Seoul, Korea*

⁴⁴*State University of New York, Stony Brook, New York 11794*

⁴⁵*Tata Institute of Fundamental Research, Colaba, Mumbai 400005, India*

⁴⁶*University of Texas, Arlington, Texas 76019*

⁴⁷*Texas A&M University, College Station, Texas 77843*

Abstract

We present a study of $Z\gamma + X$ production in $p\bar{p}$ collisions at $\sqrt{s} = 1.8$ TeV from 97 (87) pb^{-1} of data collected in the $ee\gamma$ ($\mu\mu\gamma$) decay channel with the DØ detector at Fermilab. The event yield and kinematic characteristics are consistent with the Standard Model predictions. We obtain limits on anomalous $ZZ\gamma$ and $Z\gamma\gamma$ couplings for form factor scales $\Lambda = 500$ GeV and $\Lambda = 750$ GeV. Combining this analysis with our previous results yields 95% CL limits $|h_{30}^Z| < 0.36$, $|h_{40}^Z| < 0.05$, $|h_{30}^\gamma| < 0.37$, and $|h_{40}^\gamma| < 0.05$ for a form factor scale $\Lambda = 750$ GeV.

Studies of vector boson pair production and measurements of the trilinear gauge boson couplings provide important tests of the Standard Model (SM) of electroweak interactions. The SM predicts no tree-level couplings between the Z boson and the photon. Observation of such couplings would indicate the presence of new physical phenomena. Recent limits on the $ZZ\gamma$ and $Z\gamma\gamma$ coupling parameters have been obtained by CDF [1], L3 [2], DELPHI [3] and DØ [4,5].

In the SM, the $\ell^+\ell^-\gamma$ final state can be produced via radiative decays of the Z boson or by production of a boson pair via t - or u -channel quark exchange. The former process is the dominant source of events with small opening angle between the photon and charged lepton and for events with a low value of photon transverse energy, E_T^γ . Events produced by the latter process have lepton-pair invariant mass, $m_{\ell\ell}$, close to M_Z and three-body invariant

mass, $m_{\ell\ell\gamma}$, larger than M_Z . Anomalous $ZZ\gamma$ or $Z\gamma\gamma$ couplings would enhance the cross section for $Z\gamma$ production, particularly for high- E_T photons, relative to the SM expectations.

A study of $Z\gamma$ production and a search for anomalous $Z\gamma$ couplings has been performed using the reactions $p\bar{p} \rightarrow ee\gamma X$ and $\mu\mu\gamma X$ at $\sqrt{s} = 1.8$ TeV in data collected with the DØ detector at Fermilab during the 1993-1995 Tevatron run. These data correspond to an integrated luminosity of 97 ± 5 (87 ± 5) pb^{-1} in the $ee\gamma$ ($\mu\mu\gamma$) channels. This study is complementary to that of Ref. [5], which sets limits on anomalous $ZV\gamma$ ($V = Z, \gamma$) couplings using a fit to the E_T^γ spectrum in events analyzed with the $Z \rightarrow \nu\bar{\nu}$ hypothesis. The sensitivities to anomalous couplings are equivalent based on the expected event yields and E_T^γ spectra. The backgrounds are dissimilar and the signal-to-background ratio is much higher in the charged-lepton analysis. Also, the kinematic characteristics of the charged-lepton events can be studied in detail.

The results of the search for anomalous couplings are presented within the formalism of Ref. [6], which assumes only that any possible trilinear $ZV\gamma$ coupling must obey Lorentz and gauge invariance. In this formalism, the most general $ZV\gamma$ vertex contains four undetermined coupling parameters h_i^V ($i = 1, \dots, 4$). Terms proportional to h_1^V and h_2^V in the scattering amplitudes are CP-odd, while those proportional to h_3^V and h_4^V are CP-even. To ensure partial wave unitarity at high energies, a form factor ansatz $h_i^V(\hat{s}) = h_{i0}^V/(1 + \hat{s}/\Lambda^2)^{n_i}$ is used [6], where $\sqrt{\hat{s}}$ is the parton center-of-mass energy, h_{i0}^V is the value of h_i^V in the low-energy limit $\hat{s} = 0$, Λ is a mass scale, and n_i is the form factor power. Form factor powers of $n_1 = n_3 = 3$ and $n_2 = n_4 = 4$ were used. These choices of n_i provide the terms in the amplitude proportional to h_i^V with same high energy behavior.

The DØ detector, described in detail in Ref. [7], consists of three main systems: the inner tracker, the calorimeter, and the muon systems. A nonmagnetic central tracking system, composed of central and forward drift chambers, provides directional information for charged particles and is used in this analysis to discriminate between electrons and photons and in muon identification. Particle energies are measured by a liquid-argon uranium sampling calorimeter that is divided into three cryostats. The central calorimeter (CC)

covers pseudorapidity $|\eta| < 1.1$, and the end calorimeters (EC) cover $1.1 < |\eta| < 4.4$. The EM (hadron) calorimeters are divided into four (four to six) layers to measure longitudinal shower development. Energy resolutions of approximately $\sigma(E)/E = 15\%/\sqrt{E} \oplus 0.4\%$ (E in GeV) are achieved for electrons and photons. The muon system consists of magnetized iron toroids with one inner and two outer layers of drift tubes and achieves a momentum resolution of $\sigma(1/p) = 0.18(p - 2)/p^2 \oplus 0.003$ with p in GeV/c.

Data were collected with a multi-level trigger system. The $ee\gamma$ candidates were required to contain two EM clusters with $E_T > 20$ GeV. The trigger efficiency was estimated to be nearly 100% for events that satisfied the offline $ee\gamma$ selection criteria given in the next paragraph. The $\mu\mu\gamma$ candidates were required to have at least one muon within $|\eta| < 1$ and $p_T > 8$ GeV/c and to have an EM cluster with $E_T > 7$ GeV. The trigger efficiency ranged from 60% to 90% depending on E_T^γ and on whether the event passed the tight or loose muon selection described below.

Events which satisfied the trigger requirements were subjected to further selection criteria. Each $ee\gamma$ event was required to have two electron candidates with $E_T > 25$ GeV and a photon candidate with $E_T > 10$ GeV within the fiducial region $|\eta| < 1.0$ (CC) or $1.5 < |\eta| < 2.5$ (EC). Of the two electron candidates, one was required to have a matching track, and the other was required to have a track or drift chamber hits associated with the electromagnetic shower. The photon was required to have no matching track and no drift chamber hits nearby.

Two samples of $\mu\mu\gamma$ candidates were identified. The events identified using the tight selection criteria were required to have a photon, and two isolated muon tracks in the region $|\eta| < 1$. The events identified using the loose selection criteria were required to have: a photon; an isolated muon track in the region $|\eta| < 1$; and a muon identified [8,9] by a pattern of isolated energy deposition in the longitudinal segments of the hadron calorimeter in the region $|\eta| < 2.4$, with an azimuth, ϕ , within 0.4 radians of the direction of the missing transverse energy corrected for the p_T of the tracked muon. In the tight selection, one muon was required to have $p_T > 15$ GeV/c and the other to have $p_T > 10$ GeV/c. In

the loose selection, the muon with a track was required to have $p_T > 15$ GeV/ c . In both selections the opening angle between the muons was required to be between 40 and 160 degrees. Also, the photon candidate was required to be within the fiducial region $|\eta| < 1.1$ (CC) or $1.5 < |\eta| < 2.5$ (EC), to have $E_T > 10$ GeV, and not to have a matching central detector track.

An angular separation of $\mathcal{R}_{\ell\gamma} \equiv \sqrt{\Delta\eta^2 + \Delta\phi^2} > 0.7$ was required between the photon and the electrons or muons. This reduces the number of radiative $Z \rightarrow \ell^+\ell^-\gamma$ decay events in the final sample while maintaining sensitivity to $ZV\gamma$ couplings.

The efficiencies for the above selection criteria were estimated using $Z \rightarrow ee$ and $Z \rightarrow \mu\mu$ candidates in the data. For electrons, the detection efficiency was measured to be about 80% when a track match was required. When only drift chamber hits were required, the efficiency increased to about 90%. Including the geometrical acceptance, the muon tracking and reconstruction efficiency was $41 \pm 2\%$ for $|\eta| < 1.0$, and $80 \pm 2\%$ ($64 \pm 3\%$) for muons identified by the calorimeter with $|\eta| < 1.1$ ($1.1 < |\eta| < 2.4$). The overall acceptance of the loose $\mu\mu\gamma$ selection criteria was 3.2 times greater than that of the tight $\mu\mu\gamma$ selection criteria. The photon efficiency was found to depend on E_T and η , and ranged from 35% for EC photons at $E_T^\gamma = 10$ GeV to approximately 70% for CC photons with $E_T^\gamma > 25$ GeV. The efficiency of the veto against photons with drift chamber hits or tracks in close proximity, used in the $ee\gamma$ analysis, ranged from 80% in the CC to 60% in the EC. The energy dependence of the photon detection efficiency, due to the effects of the underlying event and noise, was estimated from photons simulated with GEANT [10] superimposed on minimum bias data collected during the run.

A parametric detector simulation [11] along with a leading-order MC event generator [6], was used to predict the signal as a function of the couplings h_{i0}^V . A K-factor of 1.34 [6] was used to correct the predicted cross section for processes not included in the leading-order calculation. Additionally, the $\ell\ell\gamma$ system was given a transverse momentum according to the theoretical prediction for Z boson production [12] to simulate kinematic effects [13] not included in the event generator. Parton densities were taken from the MRSD- $'$ set [14].

A total theoretical uncertainty of 6% is assigned to the signal prediction. This uncertainty reflects the variation in predicted signal for Q^2 scales in the range $\hat{s}/4 < Q^2 < 4\hat{s}$ using recently fitted parton densities.

With an integrated luminosity of 97 (87) pb^{-1} , the expected SM $ee\gamma$ ($\mu\mu\gamma$) signal is 13.2 ± 1.3 (16.3 ± 2.0) events. The contributions to the systematic uncertainty on this prediction, listed in Table 1, total 10% (12%).

The major source of background in the electron decay channel is Z +jets production with a jet misidentified as a photon. Contributions from multijet and direct photon (γ + jets) processes in which one or more jets are misidentified as an electron or photon are smaller but not negligible. Similarly, the major background for the muon decay channel is Z +jets production. The sample selected with the loose selection criteria also includes substantial background from W +jets with a fake muon and a jet misidentified as a photon.

The probability for a jet to be misidentified as a photon was measured from an independent sample of multijet events. After subtracting the expected number of direct photons in the sample, the misidentification probability $P_{j \rightarrow \gamma}$ was found to depend slightly on E_T^{jet} and was estimated to be $\sim 10^{-3}$. A systematic uncertainty of 25% assigned to $P_{j \rightarrow \gamma}$ accounts for the uncertainty in the direct photon fraction of the multijet sample. The electron misidentification probability $P_{j \rightarrow e}$ was measured in a similar way and was found to be about half of $P_{j \rightarrow \gamma}$. The backgrounds in the $ee\gamma X$ and $\mu\mu\gamma X$ candidate samples were estimated by weighting $eejX$, $\mu\mu jX$, and $e\gamma jX$ events in the parent sample by the appropriate $P_{j \rightarrow \gamma}$ and $P_{j \rightarrow e}$ factors. The background from events with jets misidentified as electrons or photons is 1.81 ± 0.54 events for the $ee\gamma$ channel, 0.29 ± 0.08 events for the tight $\mu\mu\gamma$ channel, and 1.89 ± 0.54 events for the loose $\mu\mu\gamma$ channel.

Contributions from processes such as $Z\gamma \rightarrow \tau^+\tau^-\gamma$ and $WZ \rightarrow \ell\ell e\nu$ were investigated and found to be negligible for the $ee\gamma$ channel and for the $\mu\mu\gamma$ channel selected with the tight criteria. However, the $\mu\mu\gamma$ sample selected with the loose selection criteria has backgrounds of 1.11 ± 0.30 events from $W\gamma \rightarrow \mu\nu\gamma + X$, 0.28 ± 0.08 events from $Z \rightarrow \tau\tau \rightarrow \mu e + X$, and 0.013 ± 0.002 events from WW and $t\bar{t} \rightarrow \mu e + X$, which arise because of a fake muon. The

probability for fake muons was measured using the $Z \rightarrow ee$ and $Z \rightarrow \mu\mu$ data.

In the data 14 (15) $ee\gamma$ ($\mu\mu\gamma$) candidate events were identified. Four of the $\mu\mu\gamma$ events were from the tight selection criteria and 11 were from the loose selection criteria. The predicted total background is 1.81 ± 0.54 (3.57 ± 0.68) events in the $ee\gamma$ ($\mu\mu\gamma$) channel. Thus, the measured signal is 12.2 ± 3.8 (11.4 ± 3.9) events. The total is consistent with the predictions of the SM, as are the contributions from the individual channels.

The kinematic distributions of the candidates are shown in Fig. 1, along with the corresponding background distributions. Figure 1(a) shows the E_T^γ spectrum of the combined electron and muon channels. The spectrum is consistent with the expectation of the SM. Figures 1(b) and 1(c) show the dielectron invariant mass and dielectron-photon invariant mass, respectively. Two $ee\gamma$ events were observed with $E_T^\gamma \approx 75$ GeV, dielectron invariant mass $M_{ee} \approx M_Z$, and dielectron-photon invariant mass $M_{ee\gamma} \approx 200$ GeV/ c^2 . Assuming SM $Z\gamma$ production, the probability of observing two or more events with $E_T^\gamma > 60$ (70) GeV in the combined electron and muon channels is 15% (7.3%). The SM Monte Carlo indicates the most likely $ee\gamma$ mass for events with E_T^γ in the range 70 to 79 GeV is 200 GeV/ c^2 . Thus the two events can be understood as a fluctuation of SM $Z\gamma$ production. Note that the dielectron mass distribution shows indications of the predicted two-peaked structure induced by the photon E_T threshold and the $e\gamma$ opening angle selection criteria used to suppress the radiative events. The number of $Z\gamma$ production candidates with $M_{ee} > 83$ GeV/ c^2 and $M_{ee\gamma} > 100$ GeV/ c^2 is consistent with the SM prediction. The plots analogous to Figs. 1(b) and 1(c) for the muon channel show agreement with the SM predictions, but the detailed structure seen in the electron channel plots is obscured by the limited momentum resolution of the muon system.

Limits on the $ZV\gamma$ couplings were extracted from the data by performing an unbinned likelihood fit to the E_T^γ distribution that utilized both the shape of the photon spectrum and the total event yield. The likelihood function was convoluted with Gaussian probability distributions to account for the systematic uncertainties. With the constraint that only one coupling be nonzero at a time (1D), the 95% confidence level (CL) limits are $|h_{30}^Z| < 1.31$,

$|h_{40}^Z| < 0.26$, $|h_{30}^\gamma| < 1.36$, and $|h_{40}^\gamma| < 0.26$ for a form factor scale $\Lambda = 500$ GeV. Contours for the 95% CL two-dimensional (2D) limits [15] on the CP-even $ZZ\gamma$ and $Z\gamma\gamma$ coupling pairs (where two of the anomalous couplings are allowed to vary at the same time) are shown in Figs. 2(a) and 2(b). With $\Lambda = 750$ GeV, the 1D limits are $|h_{30}^Z| < 0.67$, $|h_{40}^Z| < 0.08$, $|h_{30}^\gamma| < 0.69$, and $|h_{40}^\gamma| < 0.08$. The 2D limits for $\Lambda = 750$ GeV are slightly looser than the unitarity constraints. The limits on the CP-odd couplings are nearly identical to the corresponding limits on the CP-even couplings. These are the most restrictive limits available from the $ee\gamma$ and $\mu\mu\gamma$ final states. Though the studies have equivalent sensitivities, limits from this analysis are less restrictive than those of Ref. [5] because of the observed event yields and E_T^γ spectra.

Combining these results with our previous measurements [4,5] yields 95% CL 1D limits

$$|h_{30}^Z| < 0.36, |h_{40}^Z| < 0.05 \quad (h_i^\gamma = 0)$$

$$|h_{30}^\gamma| < 0.37, |h_{40}^\gamma| < 0.05 \quad (h_i^Z = 0)$$

for $\Lambda = 750$ GeV. These combined limits are 20% tighter than the previous most restrictive combined limits [16]. Figures 2(c) and 2(d) show the two-dimensional limits on the $ZZ\gamma$ and $Z\gamma\gamma$ couplings from the combined analyses.

In conclusion, a search for anomalous Z -photon couplings was performed by studying $ee\gamma X$ and $\mu\mu\gamma X$ production using the DØ detector. A total of 14 (15) $ee\gamma X$ ($\mu\mu\gamma X$) candidate events were observed, in agreement with the 13.2 ± 1.3 (16.3 ± 2.0) signal events predicted by the SM and the expected background of 1.81 ± 0.54 (3.57 ± 0.68) events. The photon transverse energy spectrum, the dilepton invariant mass, and the $\ell\ell\gamma$ invariant mass are as expected from the predictions of the SM and provide evidence of $Z\gamma$ pair production. Limits on anomalous $ZZ\gamma$ and $Z\gamma\gamma$ couplings were derived. These results, combined with our previous measurements, provide the most stringent constraints on anomalous $ZZ\gamma$ and $Z\gamma\gamma$ couplings available.

We thank U. Baur for providing the MC event generator and helpful discussions. We thank the staffs at Fermilab and collaborating institutions for their contributions to this

work, and acknowledge support from the Department of Energy and National Science Foundation (U.S.A.), Commissariat à L'Energie Atomique (France), State Committee for Science and Technology and Ministry for Atomic Energy (Russia), CNPq (Brazil), Departments of Atomic Energy and Science and Education (India), Colciencias (Colombia), CONACyT (Mexico), Ministry of Education and KOSEF (Korea), and CONICET and UBACyT (Argentina).

REFERENCES

* Visitor from Universidad San Francisco de Quito, Quito, Ecuador.

† Visitor from IHEP, Beijing, China.

- [1] CDF Collaboration, F. Abe *et al.*, Phys. Rev. Lett. **74**, 1941 (1995).
- [2] L3 Collaboration, P. Acciarri *et al.*, Phys. Lett. B **346**, 190 (1995).
- [3] DELPHI Collaboration, P. Abreu *et al.*, Phys. Lett. B **380**, 471 (1996).
- [4] DØ Collaboration, S. Abachi *et al.*, Phys. Rev. Lett. **75**, 1028 (1995).
- [5] DØ Collaboration, S. Abachi *et al.*, Phys. Rev. Lett. **79**, 3640 (1997).
- [6] U. Baur and E. Berger, Phys. Rev. D **47**, 4889 (1993).
- [7] DØ Collaboration, S. Abachi *et al.*, Nucl. Instrum. and Methods A **388**, 185 (1993).
- [8] T. Fahland, Ph. D. thesis, Brown University, 1996 (unpublished). This muon identification algorithm was used to veto events with a second muon in the $W\gamma \rightarrow \mu\nu\gamma$ analysis. We improved the algorithm by requiring that the total energy deposited in the calorimeter by the muon candidate be at least 1.0 GeV for $|\eta| < 1.1$ and at least 2.0 GeV for $1.1 < |\eta| < 2.4$.
- [9] DØ Collaboration, S. Abachi *et al.*, Phys. Rev. Lett. **78**, 3634 (1997).
- [10] F. Carminati *et al.* “GEANT Users Guide v3.14,” CERN Program Library, December 1991 (unpublished).
- [11] S. Glenn, Ph.D. thesis, University of California at Davis, 1996 (unpublished).
- [12] G. Ladinsky and C.P. Yuan, Phys. Rev. D **50**, 4239 (1994).
- [13] J. Ohnemus, Phys. Rev. D **51**, 1068 (1995).
- [14] A. Martin, W. Stirling, and R. Roberts, Phys. Lett. B **306**, 145 (1993).

- [15] The one- and two-dimensional 95% CL contours correspond to log-likelihood function values 1.92 and 3.00 below the maximum.
- [16] DØ Collaboration, S. Abachi *et al.*, Fermilab-Pub-97/088-E, accepted for publication in Phys. Rev. D (1997).

FIGURES

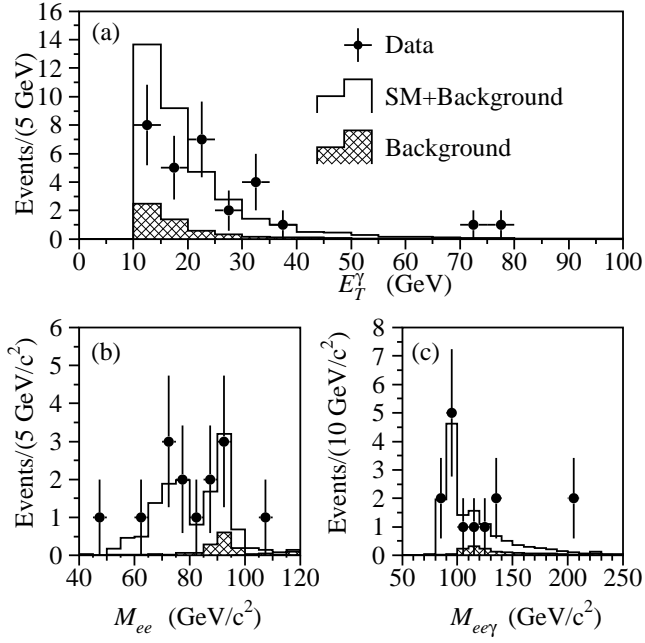


FIG. 1. Kinematic distributions for candidates and background estimates: (a) photon transverse energy for the combined $ee\gamma$ and $\mu\mu\gamma$ samples, (b) dielectron invariant mass, (c) dielectron-photon invariant mass.

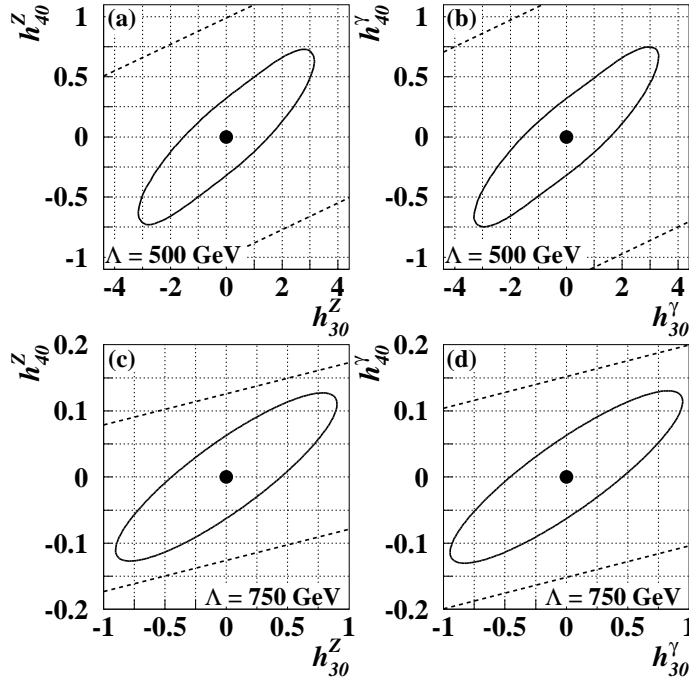


FIG. 2. Two-dimensional limits (a) on h_{30}^Z vs. h_{40}^Z , and (b) on h_{30}^γ vs. h_{40}^γ from the $ee(\mu\mu)\gamma$ analyses and the same, (c) and (d), from combining this analysis with previous results from this experiment. Only the couplings varied in each plot are assumed to be different from the SM values. Unitarity limits are indicated by the dashed contours.

TABLES

Channel	$ee\gamma$	$\mu\mu\gamma$
PDF choice, Q^2 , k -factor	6%	6%
$p_T^{ll\gamma}$	1%	1%
$ll\gamma$ selection efficiency	2.3%	6.3%
Photon conversion rate	5%	5%
Random overlap rate	3%	3%
Luminosity	5.3%	5.3%
Total:	10%	12%

TABLE I. Summary of the systematic uncertainties for the predicted $p\bar{p} \rightarrow ee\gamma$ and $\mu\mu\gamma$ signals.